Self-assembly of a Model Peptide incorporating a Hexa-Histidine sequence attached to an Oligo-Alanine sequence, and binding to Gold NTA/Nickel nanoparticles

Article

pubs.acs.org/Biomac

Self-Assembly of a Model Peptide Incorporating a Hexa-Histidine Sequence Attached to an Oligo-Alanine Sequence, and Binding to Gold NTA/Nickel Nanoparticles

Ian W. Hamley,* Steven Kirkham, Ashkan Dehsorkhi, and Valeria Castelletto†

Department of Chemistry, University of Reading, Whiteknights, Reading RG6 6AD, United Kingdom

Jozef Adamcik and Raffaele Mezzenga

Food and Soft Materials Science, ETH Zürich, Schmelzbergstrasse 9, 8092 Zürich, Switzerland

Janne Ruokolainen

Department of Applied Physics, Aalto University School of Science, P.O. Box 15100, FI-00076 Aalto, Finland

Claudia Mazzuca, Emanuela Gatto, and Mariano Venanzi

Department of Chemical Sciences and Technologies, University of Rome "Tor Vergata", Via Ricerca Scientifica 1, 00133 Rome, Italy

Ernesto Placidi

Institute of Structure of Matter, CNR, Department of Physics, University of Rome "Tor Vergata", 00133 Rome, Italy

Panayiotis Bilalis and Hermis Iatrou

University of Athens, Department of Chemistry, Panepistimiopolis Zografou, 157 71 Athens, Greece

Supporting Information

ABSTRACT: Amyloid fibrils are formed by a model surfactant-like peptide $(Ala)_{10}$-$(His)_6$ containing a hexa-histidine tag. This peptide undergoes a remarkable two-step self-assembly process with two distinct critical aggregation concentrations (cac's), probed by fluorescence techniques. A micromolar range cac is ascribed to the formation of prefibrillar structures, whereas a millimolar range cac is associated with the formation of well-defined but more compact fibrils. We examine the labeling of these model tagged amyloid fibrils using Ni-NTA functionalized gold nanoparticles (Nanogold). Successful labeling is demonstrated via electron microscopy imaging. The specificity of tagging does not disrupt the β-sheet structure of the peptide fibrils. Binding of fibrils and Nanogold is found to influence the circular dichroism associated with the gold nanoparticle plasmon absorption band. These results highlight a new approach to the fabrication of functionalized amyloid fibrils and the creation of peptide/nanoparticle hybrid materials.

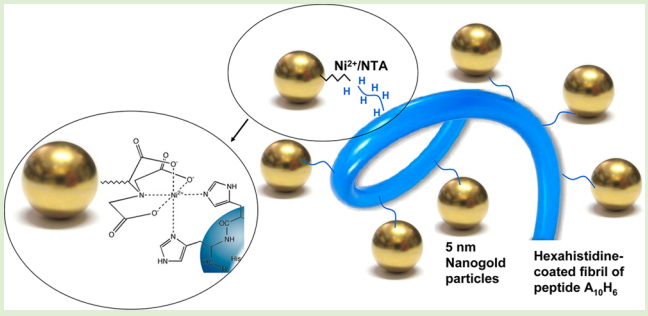

INTRODUCTION

The hexa-histidine tag, developed by researchers at Roche,[1] is widely used in the affinity purification of expressed recombinant proteins.[2] The protein to be labeled is engineered to incorporate N- or C-terminal histidine repeats. A common system employs a hexahistidine tag along with a metal chelate among which the nitrilotriacetic acid (NTA)/Ni^{2+} system is widely used. Since nickel ions are hexa-coordinated and four electrons are used in binding to NTA, two electrons are available to bind hexahistidine tags. This interaction has high

Received: July 1, 2014
Revised: August 4, 2014
Published: August 8, 2014

Scheme 1. Concept of Nanogold-Decorated Amyloid Fibrils with Hexahistidine Exterior

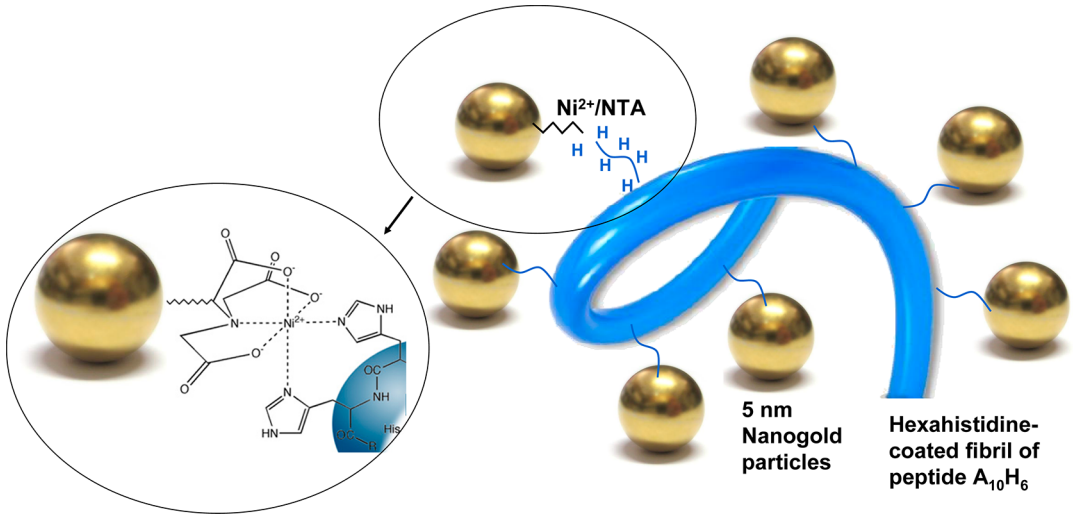

affinity and selectivity.[3−5] NTA/nickel functionalized nanoparticles termed Nanogold are available commercially for the decoration of hexahistidine-tagged proteins for transmission electron microscopy (TEM) imaging,[6,7] and this has been used to image a variety of protein complexes. The interaction of hexahistidine-tagged proteins (derived from the cartilage oligomeric matrix protein (C) coiled-coil domain, His6-C) with divalent metal ions has been investigated.[8] Binding to Zn^{2+} confers enhanced helical structure and stability, while Ni^{2+} promotes aggregation. To our knowledge, this high affinity labeling technique has not been employed to image protein or peptide "amyloid" fibrils. Amyloid refers to the formation of β-sheet rich fibrillar aggregates by peptides or proteins which results from misfolding induced by partial denaturation.

Prior work shows that organic nanoparticles (NPs) can influence amyloid fibrillization, potentially either inhibiting or accelerating fibrillization, dependent on the nature of the interaction of the peptide with the nanoparticle surface.[9] Inorganic nanoparticles such as CdSe/ZnS quantum dots have been used to label amyloid-forming peptides to probe the fibril formation or disruption process.[10−12] The interaction of gold NPs with amyloid fibrils has been examined, and in general inclusion of these nanoparticles appears to disfavor amyloid formation. In many cases, however, the NPs have a specific coating, which may be useful in applications including immune adjuvants (since the NPs can stimulate a macrophage response)[13] or in disrupting fibrillization[14−17] which may reduce amyloid cytotoxicity for ultimate therapeutic applications.[9] Recently, amyloid−metal nanoparticle conjugates for controlled transport in living cells and therapeutics have been proposed.[18] Localized heating using microwave irradiation of gold NPs can also induce amyloid fibril disassembly.[19,20] In some cases, gold NPs can induce aggregation, an effect ascribed to the presence of misfolded proteins at the nanoparticle surface.[21] In all of these prior studies, however, specific binding interactions between the amyloid peptide and the gold NPs were not utilized. Very recently, curli amyloid fibrils expressed by *E. coli* with a histidine tag have been tagged with Ni-NTA Nanogold.[22] Matsui and co-workers investigated the use of histidine-rich peptide to produce gold nanowires.[23] The histidine-rich peptide AHHAHHAAD was deposited onto nanowires formed by the amphiphile heptane dicarboxylate. The immobilization of the peptide on the nanowires facilitates subsequent coating with gold via reduction of a gold salt.

In the present paper, we investigate the possibility to decorate model "amyloid" fibrils containing the high affinity hexa-histidine tag with Ni-NTA gold nanoparticles termed "Nanogold". The first part of the Article describes the self-assembly properties of the peptide $(Ala)_{10}$-$(His)_6$, $A_{10}H_6$, and this is then followed by our results which show that the nanoparticles do not disrupt fibrillization, and thus that it is possible to successfully decorate amyloid-like fibrils with the gold nanoparticles. It has very recently been shown that gold nanoparticles coated with thiol or citrate functionalities can be coated with histidine-tagged proteins,[24] and Nanogold has been used to tag histidine-tagged proteins, for enhanced TEM imaging.[7] In contrast to this work, our research involves the specific histidine/Ni-NTA binding motif and employs model amyloid-forming peptides. In contrast to the work of Matsui et al.,[23] we did not require additional amphiphiles as templates to create peptide nanofibrils, since these are formed directly by $A_{10}H_6$.

EXPERIMENTAL SECTION

Synthesis of Alanine$_{10}$-Histidine$_6$ ($A_{10}H_6$) Oligopeptides. Boc-His(Trt)-OH was obtained from Christof Senn Laboratories (>99%), and alanine from Aldrich (97%). Dimethylamine (DMA, >99.9%, Aldrich, bp 7 °C) was condensed under high vacuum at −78 °C and was treated with sodium hydroxide pellets at room temperature for 1 day, and was subsequently distilled into precalibrated ampules with break-seals. It was then diluted with *N*,*N*′-dimethylformamide (DMF) to the appropriate concentration in a sealed apparatus equipped with precalibrated ampules and kept away from light. Thionyl chloride (99.7%, Acros Organics) was distilled prior use. Triphosgene (99%) was purchased from Acros Organics and used as received. Triethylamine (>99%, Acros Organics) was dried over calcium hydride for 1 day and then distilled and stored in the vacuum line over sodium. Ethyl acetate (>99.5%, Merck) was fractionally distilled over phosphorus pentoxide. Hexane (>99%, Merck) was distilled over sodium. Purification of tetrahydrofuran (THF, dried, max 0.005% water, Merck) was performed using standard high vacuum techniques reported elsewhere.[25] DMF (Fisher 99.9+ %, special grade for peptide synthesis with less than 50 ppm of active impurities) was further purified by short-path fractional distillation under high vacuum. The middle fraction was always used.

Synthesis of N^{im} Trityl Protected *N*-Carboxyanhydride of L-Histidine (Trt-His-NCA). The synthesis of Trt-His-NCA was

dx.doi.org/10.1021/bm500950c | *Biomacromolecules* 2014, 15, 3412−3420

performed in two steps as previously reported.[26] In the first step, the HCl salt of Trt-His-NCA was synthesized, followed by removal of the HCl to produce the pure Trt-His-NCA monomer. Briefly, 20 g (40.2 mmol) of Boc-His(Trt)-OH was added and dried overnight under high vacuum. Then 150 mL of THF was distilled in the flask, giving a clear yellowish solution. The reaction flask was placed in an ice-bath, filled with argon, and 3.25 mL (44.2 mmol) of thionyl chloride diluted in 20 mL of THF was added dropwise in a period of 10 min. By the end of addition of thionyl chloride, the solution became yellowish. After 2 h, the solution was poured into 2 L of cold $(Et)_2O$ with precipitation of Trt-His-NCA·HCl as the major product. The solid was filtered and then transferred to a round-bottom flask. Next, 300 mL of ethyl acetate was distilled and the mixture was placed into a water bath, at 45 °C for 1 h, resulting in dissolution. Then the solution was cooled to 0 °C with an ice bath and Trt-His-NCA·HCl was formed as a precipitate which was isolated as the only product after filtration (12.5 g, 28 mmol).

In the second step, 200 mL of ethyl acetate was distilled to the above solid and the suspension was placed in an ice bath. A solution of 50 mL ethyl acetate with an equimolar amount of triethylamine (3.5 mL, 28 mmol) was slowly added dropwise under vigorous stirring (duration of addition 1 h). The resulting triethylamine hydrochloride was filtered off, and the filtrate was poured into 1.5 L of nonsolvent hexane in order to recrystallize the Trt-His-NCA. A second recrystallization occurred with a mixture of solvent/nonsolvent ethyl acetate/hexane (1:5), and the white solid was isolated by filtration. Finally, Trt-His-NCA was dried under vacuum overnight (11.05 g, 27 mmol, 67% yield).

Synthesis of *N*-Carboxy Anhydride of L-Alanine (Ala-NCA). The synthesis process of the Alanine NCA (Ala-NCA) was accomplished according to a previously published method.[27] Briefly, Ala-NCA was synthesized from the corresponding L-α-amino acid and triphosgene in acetonitrile (suspension) at 70 °C, under an inert atmosphere. The unreacted species along with the amino acid salts (insoluble species) were removed by filtration. Ala-NCA was subsequently dissolved and dried several times with ethyl acetate under high vacuum, in order to remove the excess triphosgene, which sublimes under high vacuum, along with the remaining HCl. Finally, Ala-NCA was dissolved in ethyl acetate and was recrystallized from *n*-hexane three times under high vacuum in a custom-made apparatus. The purified NCA was stored under an inert atmosphere at 0 °C.

Synthesis of $A_{10}H_6$ Oligopeptide. Polymerization was carried out with dimethylamine as the initiator. The sequential addition methodology was used for the synthesis of the oligopeptide. In a solution of Ala-NCA in DMF (6 mL, ~10% w/w), 5.2×10^{-4} mol dimethylamine was added. After the completion of polymerization (2 days), Trt-His-NCA (1.31 g, 3.1×10^{-3} mol) was then added and was left to react until all monomer was completely consumed. After complete consumption of Trt-His-NCA (4 days), a small aliquot of the raw product was removed from the reactor for characterization and control of the completion of the polymerization. The final oligopeptide was precipitated in diethyl ether, filtered, and dried to constant weight.

For the deprotection of trityl groups, the oligopeptide was suspended in CH_2Cl_2 (20% w/v) and an equal volume of trifluoroacetic acid (TFA) was added. The polymer was completely dissolved and was left to be deprotected for 1 h at room temperature, and the solution became yellowish-light brown. Subsequently, an equimolar amount of triethyl silane was added (in respect to the number of His monomeric units), and the solution from yellowish-light brown turned colorless. The solution was poured in diethyl ether, and the white solid was filtered and dried. The reactions used are shown in Supporting Information Scheme 1.

Characterization of Synthesized Oligopeptide. A special set of columns for low molecular weight samples were used to characterize the oligomers. The size exclusion chromatography (SEC) system comprised of a Waters 600 high pressure liquid chromatographic pump, Waters HT columns, a Waters 410 differential refractometer detector, and a Precision PD 2020 two angles (15°, 90°) light scattering detector. A 0.1 N LiBr DMF solution was used as an eluent at a rate of 1 mL/min at 60 °C. The SEC chromatograms obtained for the A_{10} precursor along with the final $A_{10}H_6$ are shown in Supporting Information Figure 1. The molecular weight of the A_{10} precursor obtained is 780 g/mol which corresponds to the 10 alanine units plus the molecular weight of the initiator. The molecular weight of the final block oligopeptide was 3050 g/mol. Consequently, the molecular weight of the protected oligohistidine block was 2270 which corresponds to 6 protected histidine units. The corresponding molecular weight of the deprotected oligohistidine in the form of TFA salt would be 1500. The deprotection of trityl groups of His segments was confirmed by the elimination of the peaks at 708 and 728 cm^{-1} in the FTIR spectra (Supporting Information Figure 2).

The composition of the oligopeptide was verified by ^1H NMR spectroscopy (Supporting Information Figure 3). ^1H NMR spectroscopy (300 MHz) was performed using a Varian Unity Plus 300/54 spectrometer. The spectra of the polymers were acquired in CF_3COOD at room temperature. The peaks used to obtain the composition were at 4.85 ppm which is the total α-protons of oligoalanine segments and the one at 5.25 ppm which is the total α-protons of the oligohistidine groups. The molar ratio between A/H groups was found to be 10/6.

Other Reagents. MOPS buffer was purchased from Sigma-Aldrich, and 5 nm Ni-NTA-Nanogold was purchased from Nanoprobes. MOPS was prepared by dissolving powder in distilled water to give a concentration of 50 mM. $A_{10}H_6$ was dissolved through vortex and bath sonication in distilled water for initial experiments, and then 50 mM MOPS at pH 7.9 was used for experiments incorporating Nanogold particles. The Nanogold particle preparation protocol indicated that His-tagged protein samples were to be preprepared in binding buffer (MOPS in this case) at pH 7−8, which was adjusted using 8.4% NaOH. This was to avoid protonation of the histidines which would affect interactions with the metal. The $A_{10}H_6$ samples were incubated with the Nanogold particles in MOPS buffer for 5−30 min at room temperature.

Steady State Fluorescence Experiments. Fluorescence spectroscopy was used to locate the critical aggregation concentration in the micromolar (cac1) and millimolar (cac2) concentration regions. Fluorescence spectra were recorded with a Varian Cary Eclipse fluorescence spectrometer with samples in 4 mm inner width quartz cuvettes. Thioflavin T (ThT) was used as a probe of amyloid fibril formation, and pyrene as a fluorophore sensitive to the hydrophobic environment. The fluorescence assays were performed using 4.9×10^{-3}−1.95 wt % $A_{10}H_6$ solutions in distilled water. The concentration of ThT used was 5.5×10^{-9} wt %, and that of pyrene was 1.3×10^{-5} wt %. For the ThT assay, spectra were measured from 460 to 600 nm using λ_{ex} = 440 nm. For the pyrene assays, spectra were measured from 360 to 550 nm using λ_{ex} = 339 and 1.5 nm slit width for both excitation and emission monochromators.

To detect cac1, the ratio of the intensities of the first (I_1, λ_{em} = 373 nm) and third (I_3, λ_{em} = 382 nm) vibrational components of the lowest energy (S_2-S_0) fluorescence emission of pyrene was monitored as a function of increasing peptide concentration in the buffer solution.[28] Measurements were carried out at 25 °C using a Fluorolog III spectrofluorimeter (HORIBA, Japan). Samples were excited at λ_{ex} = 310 nm, and emission was recorded in the 350−450 nm spectral range. Experiments were performed at two different pH values, that is, at pH = 7.6 and pH = 4.4. In the first case, a Tris buffer ([Tris] = 25 mM, [NaCl] = 150 mM) was used, while in the second case a phosphate buffer ($[NaH_2PO_4]$ = 25 mM, [NaCl] = 150 mM) was used. The dye concentration was 4×10^{-5} wt % (2 μM), while the peptide concentration varied from 0 to 0.007 wt % (100 μM). Peptide was added from a concentrated methanol stock solution; the final dilution was below 5%.

Time Resolved Fluorescence Experiments. To determine the aggregation number at micromolar concentration, the fluorescence decay of pyrene ([pyrene] = 2 μM; excitation: λ_{ex} = 344 nm, emission: λ_{em} = 400 nm) was progressively quenched by the water-insoluble quencher, *N*,*N*′-dibutyl aniline (DBA).[29] The quencher was introduced in microliter aliquots of a concentrated ethanol solution in the concentration range 0−50 μM. To investigate the dependence

of the aggregation number on the peptide concentration, measurements were performed with $[A_{10}H_6]$ = 226 μM and $[A_{10}H_6]$ = 400 μM. Experiments were performed in Tris buffer ([Tris] = 25 mM, [NaCl] = 150 mM, pH = 7.6). Fluorescence decays were measured using a Lifespec ps, SPC lifetime apparatus (Edinburgh Instruments, U.K.). Excitation was achieved by using a diode (λ_{ex} = 344 nm, pulse duration <1 ns) at λ_{em} = 400 nm. The experimental time decays were fitted through an iterative reconvolution procedure assuming that the fluorescence intensity time decay of the probe (pyrene) in the presence of the quencher (DBA) was accounted for by the equation:[30]

$$I(t) = I(0)(\exp\{-t/\tau_0 - C[1 - \exp(-k_q t)]\}) \quad (1)$$

where τ_0 is the time decay of the probe (measured separately under the same experimental conditions, but in the absence of quencher molecules), k_q is the quenching rate constant, and C is the average number of quenchers per aggregate. This equation assumes that the fluorescence lifetime of the probe is much shorter than its residence time in the hydrophobic core of the peptide aggregate. The aggregation number (N) is then obtained using the equation:[31]

$$N = ([P] - \text{cac1})C/[DBA] \quad (2)$$

where [P] is the peptide molar concentration, [DBA] is the molar concentration of the quencher, and cac1 is the critical concentration for the formation of prefibrillar aggregates.

Gold Nanoparticle UV/Vis Absorption Spectroscopy. Absorption measurements were carried out using a Cary 100 SCAN (Varian, Palo Alto, CA) spectrophotometer. The Ni-NTA gold nanoparticle solution (0.5 μM) was diluted 1:5 (v/v) with MOPS buffer (50 mM). The experiment was carried out in a quartz cell of 1.0 cm path length.

Circular Dichroism (CD). For secondary structure measurements, spectra for samples solutions in MOPS buffer made up in D_2O (the same samples being used for FTIR experiments) were recorded using a Chirascan spectropolarimeter (Applied Photophysics, U.K.). The sample was placed in a coverslip cuvette (0.1 mm thick). Spectra are presented with absorbance $A < 2$ at any measured point with a 0.5 nm step, 1 nm bandwidth, and 1 s collection time per step at 20 °C. The post-acquisition smoothing tool from Chirascan software was used to remove random noise elements from the averaged spectra. A residual plot was generated for each curve in order to verify whether the spectrum has been distorted during the smoothing process. The CD signal from MOPS buffer was subtracted from the CD data of the peptide solutions.

For dichroism studies of the histidine-gold nanoparticle interaction in the visible region, CD experiments were performed using a Jasco J600 spectrometer (Jasco, Tokyo, Japan) using quartz cuvettes of 1 cm path length. For each spectrum, eight scans were recorded. Aliquots of $A_{10}H_6$ solutions (72 μM, i.e., above cac1, and 7 μM, i.e., below cac1) were added to 0.1 μM Ni-NTA gold nanoparticles in MOPS at pH 7.9.

Fourier Transform Infrared (FTIR) Spectroscopy. Spectra were recorded for samples dissolved in MOPS buffer made up in D_2O using a Thermo Scientific Nicolet IS5 or a Nexus-FTIR spectrometer, both equipped with a DTGS detector. Samples of around 10−20 μL were placed between two CaF_2 plates with a 0.0012 mm thick spacer in between, and loaded into an Omnicell holder (Specac). Spectra were scanned 128 times over the range of 900−4000 cm^{-1}.

Small-Angle X-ray Scattering (SAXS). Experiments were performed on beamline BM29 at the ESRF (Grenoble, France). A few microlitres of samples were injected via an automated sample exchanger at a slow and very reproducible flux into a quartz capillary (1.8 mm internal diameter), which was then placed in front of the X-ray beam. The quartz capillary was enclosed in a vacuum chamber, in order to avoid parasitic scattering. After the sample was injected in the capillary and reached the X-ray beam, the flow was stopped during the SAXS data acquisition. The sample was thermostated throughout its entire travel from the injector to the quartz capillary. SAXS experiments were performed at 20 °C. The $q = 4\pi \sin\theta/\lambda$ range is approximately 0.04−5 nm^{-1}, with λ = 1.03 Å (12 keV) and a 2.87 m sample−detector distance. The images were captured using a PILATUS 1 M detector. Data processing (background subtraction, radial averaging) was performed using dedicated beamline software ISPYB.

Cryo-Transmission Electron Microscopy (cryo-TEM). Experiments were carried out using a field emission cryo-electron microscope (JEOL JEM-3200FSC) operating at 200 kV. Images were taken using bright-field mode and zero loss energy filtering (omega type) with a slit with 20 eV. Micrographs were recorded using a Gatan Ultrascan 4000 CCD camera. The specimen temperature was maintained at −187 °C during the imaging. Vitrified specimens were prepared using an automated FEI Vitrobot device using Quantifoil 3.5/1 holey carbon copper grids with 3.5 μm hole sizes. Grids were cleaned using a Gatan Solarus 9500 plasma cleaner just prior to use and then transferred into an environmental chamber of the FEI Vitrobot at room temperature and 100% humidity. Thereafter, 3 μL of sample solution at 2 wt % concentration was applied on the grid, blotted once for 1 s, and then vitrified in a 1/1 mixture of liquid ethane and propane at −180 °C. Grids with vitrified sample solutions were maintained in a liquid nitrogen atmosphere and then cryo-transferred into the microscope.

Transmission Electron Microscopy (TEM). TEM imaging was performed using a Philips CM20 transmission electron microscope operated at 200 kV. Droplets of solutions were placed on Cu grids coated with a carbon film (Agar Scientific, U.K.), stained with 1 wt % uranyl acetate, and air-dried.

X-ray Diffraction (XRD). X-ray diffraction was performed on a peptide stalk prepared by drawing a fiber of a 6% peptide solution between the ends of wax-coated capillaries, after separation and drying a stalk was left on the end of one capillary. The capillary was mounted vertically onto the four axis goniometer of a RAXIS IV++ X-ray diffractometer (Rigaku) equipped with a rotating anode generator. The XRD data was collected using a Saturn 992 CCD camera. The sample-to-detector distance was 50 mm.

Dynamic Light Scattering (DLS). Experiments were performed using an ALV CGS-3 system with 5003 multidigital correlator. The light source was a 20 mW He−Ne laser, linearly polarized, with λ = 633 nm. The scattering angle θ = 90° was used for all the experiments.

Samples were loaded into standard 0.5 cm diameter cylindrical glass cells. DLS experiments measured the intensity correlation function of the radiated light $g^{(2)}(q,t)$:[32]

$$g^2(q, t) = 1 + A[g^{(1)}(q, t)]^2 \quad (3)$$

where A is an instrumental correction factor, $q = [4\pi n \sin(\theta/2)]/\lambda$ is the scattering vector (λ = vacuum wavelength of the radiation and n = refractive index of the medium), t is the delay time, and $g^{(1)}(q,t)$ is the electric field correlation function. The program CONTIN can be used to determine the relaxation rate distribution of the system[33] by modeling of the field correlation function according to

$$g^{(1)}(t) = \int_0^\infty G(\Gamma) \exp(-\Gamma t)\, d\Gamma \quad (4)$$

where $G(\Gamma)$ is the relaxation rate distribution. CONTIN allows for the inverse Laplace transform in eq 4 and provides a tool for calculating the size distribution of the system ($G(R_H)$; R_H = hydrodynamic radius). R_H is taken as the radius corresponding to the maximum in $G(R_H)$.

Atomic Force Microscopy (AFM). A 20 μL of solution (0.5 wt % solution of $A_{10}H_6$ with Nanogold in MOPS) was deposited onto freshly cleaved mica, incubated for 2 min, rinsed with Milli-Q water (ρ = 18 MΩ cm^{-1}), and dried by air. Tapping mode AFM was carried out on a Nanoscope 8 multimode scanning force microscope (Bruker). AFM cantilevers (Bruker) for use in soft tapping conditions were used at a vibrating frequency of 150 kHz. Images were simply flattened using the Nanoscope 8.1 software, and no further image processing was carried out.

Additional AFM measurements on peptide films dried on a mica surface were performed in air using a Veeco Multiprobe IIIa (Santa Barbara, CA) instrument. Experiments were carried out at room temperature (20 °C) in the tapping mode by using NanoSensors SiO_2 tips with a force constant of about 40 N m^{-1} and a typical tip curvature radius of 7 nm. An aliquot of 35 μL of the peptide sample (357 μM)

dx.doi.org/10.1021/bm500950c | Biomacromolecules 2014, 15, 3412−3420

was deposited onto a freshly cleaved mica surface and left to dry completely in air before imaging. In the case of the mixed solution peptide (250 μM) and Nanogold (0.02 μM), 10 μL of the solution was deposited onto a freshly cleaved mica surface and left to dry completely in air before imaging.

RESULTS

We assessed the presence of critical aggregation concentrations using fluorescence assays with both pyrene and Thioflavin T. Pyrene is a fluorophore sensitive to the local hydrophobic environment,[28,34] and has been used previously to determine the cac for peptide systems.[35−38] Thioflavin T is used as an amyloid-specific dye.[36,37] Assays using two types of dye were performed, which revealed two separate aggregation processes. We found that a critical aggregation concentration exists in the micromolar concentration (cac1) range above which the peptide $A_{10}H_6$ self-assembles. The concentration-dependence of is the I_1/I_3 fluorescence intensity ratio of pyrene shown in Figure 1.

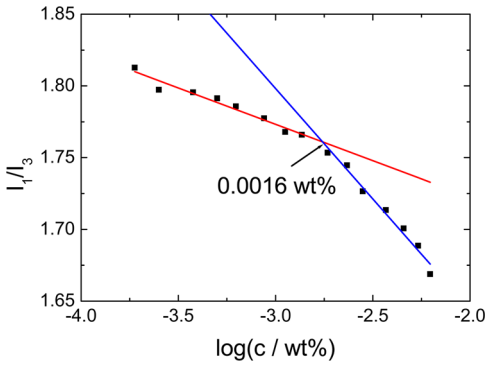

Figure 1. Pyrene fluorescence assay to determine the critical aggregation concentration in the micromolar range (cac1) of $A_{10}H_6$. I_1 and I_3 are the fluorescence intensities measured at λ_{em} = 373 and 382 nm, respectively.

Pyrene fluorescence measurements led to a value for the cac1 of 0.0016 wt % (23 μM) at pH 7.6 as shown in Figure 1. The fluorescence spectra from which the data reported in Figure 1 were obtained are reported in the Supporting Information (Figure 4). The corresponding value for cac1 at pH 4.4 was 18 μM (Supporting Information Figure 5), suggesting that the aggregation process leading to the formation of prefibrillar aggregates is rather pH-independent, at least in this pH interval.

At much higher concentration, Thioflavin T spectroscopy, supported by pyrene fluorescence measurements, reveals a separate critical concentration (cac2) for fibril formation. This is confirmed by the data in Figure 2. The two techniques reveal a critical concentration of 0.5 wt % (ThT) and 0.16 wt % (pyrene), corresponding to a cac2 = 2 mM. The difference in values obtained from the two techniques may reflect the distinct processes probed by these two dyes, that is, amyloid formation in the case of ThT and hydrophobic sequestration in the case of pyrene. The pH for the peptide around cac2 was measured as pH 2.75 for an 0.5 wt % solution and pH 2.72 for a 1 wt % solution. These concentration for cac2 is much higher than that observed for cac1 in the micromolar concentration range (Figure 1). The former can tentatively be ascribed to the formation of prefibrillar structures (vide infra). The local change in polarity probed by pyrene fluorescence presumably corresponds to the sequestration of the hydrophobic alanine

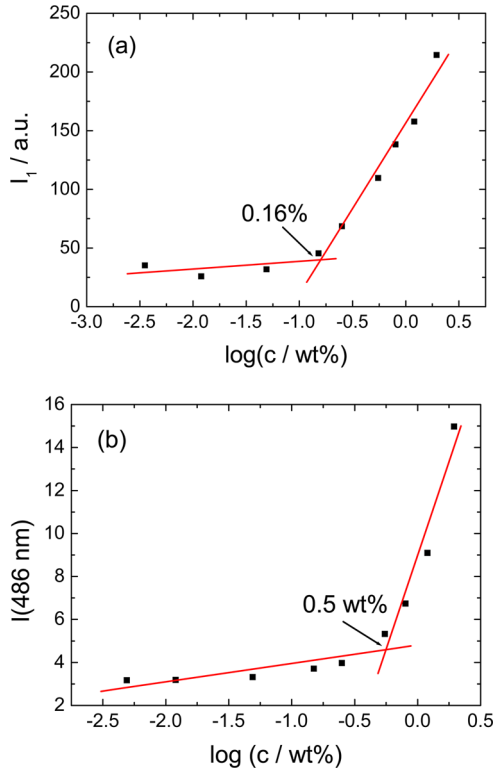

Figure 2. Assays to determine the critical aggregation concentration (cac2) of $A_{10}H_6$. (a) Pyrene fluorescence I_1 (measured at 373 nm) and (b) thioflavin T fluorescence (measured at 485 nm).

residues into the aggregate core. As described by eq 2, it was possible to determine the association number of the micelle-like aggregates from time-resolved pyrene fluorescence quenching as described in the Experimental Section. A representative fluorescence decay curve is shown in Supporting Information Figure 6. An aggregation number $N = (30 \pm 3)$ was determined for a 150 μM solution, whereas $N = (81 \pm 4)$ was obtained from a 400 μM solution. The concentration-dependent values of N show that the formation of prefibrillar aggregates is a partially open equilibrium process, since N continues to increase above cac1 (but well below cac2 for fibril formation).

The combination of ThT fluorescence with pyrene fluorescence thus seems to reveal a remarkable two-step aggregation process for $A_{10}H_6$, that is, the formation of prefibrillar aggregates at micromolar concentration, followed by a critical aggregation concentration associated with the formation of more compact fibrils (vide infra) at a millimolar peptide concentration.

We next examined the influence of gold nanoparticles on the secondary structure of the peptide. The gold nanoparticles were sized using several methods. UV/vis spectroscopy (Supporting Information Figure 7) shows a plasmon absorption maximum at 516 nm, which is consistent with 5 nm radius nanoparticles.[39] From dynamic light scattering, a hydrodynamic radius of 4.3 nm was obtained. TEM imaging (vide infra) revealed a similar size. These values of particle size can be considered to be the same within experimental uncertainties.

Spectroscopic methods all confirm that the addition of gold NPs does not influence the secondary structure of the peptide. This is shown through CD and FTIR spectroscopy, typical results being shown in Figure 3. The CD spectra (Figure 3a) show a positive peak near 200 nm with a negative band

dx.doi.org/10.1021/bm500950c | Biomacromolecules 2014, 15, 3412−3420

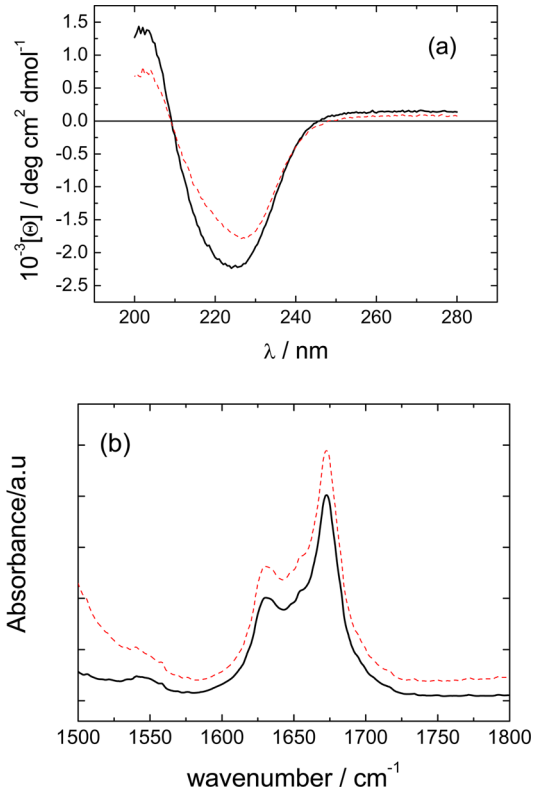

Figure 3. (a) CD spectra from 0.5 wt % solution of $A_{10}H_6$ without (solid black line) and with (dashed red line) Nanogold. (b) FTIR spectra (in deuterated buffer) of 3 wt % solution of $A_{10}H_6$ without (solid black line) and with (dashed red line) Nanogold.

centered at 225 nm. These features are consistent with β-sheet secondary structure.[40−42] The position of the minimum in the spectra is red-shifted from the usual location (216 nm) for β-sheet structures, most probably due to light scattering resulting from fibril aggregation.[43] The FTIR spectra in the amide I′ region shown in Figure 3b contain peaks at 1631 and 1672 cm^{-1}. The former peak is assigned to β-sheet structure,[41,44] while the latter is due to TFA counterion binding to the peptide.[45−47]

The formation of fibrils by $A_{10}H_6$ above cac2 is confirmed by SAXS and TEM. Figure 4 shows a cryo-TEM image which

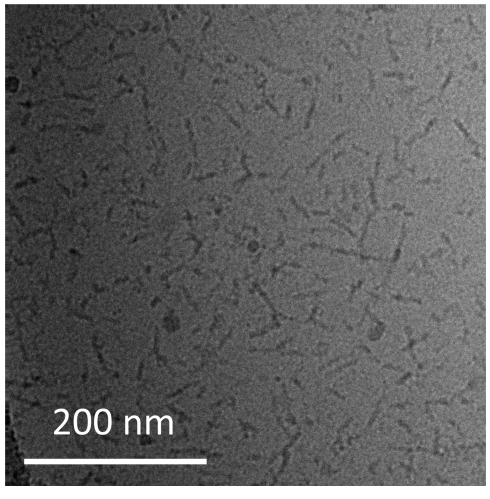

Figure 4. Cryo-TEM image from a 1 wt % solution of $A_{10}H_6$.

reveals the presence of short fibrils (variable length, but not longer than 100 nm), with a diameter of 5−10 nm. Figure 5

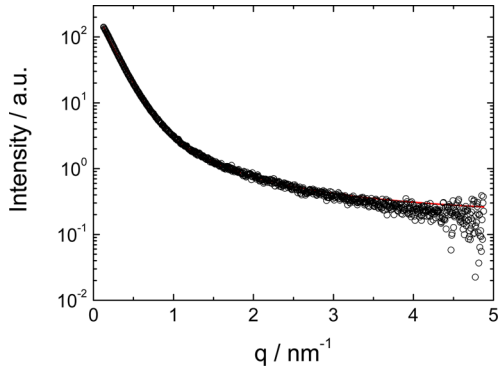

Figure 5. SAXS profile from a 0.5 wt % solution of $A_{10}H_6$ (open circles), along with core−shell cylinder form factor model fit (red line).

shows the SAXS intensity profile for a 0.5 wt % solution of $A_{10}H_6$. The scattering data can be fitted to the form factor of a core−shell cylinder,[48] corresponding to cylinders with a dense alanine-rich core and a hydrated histidine-rich corona. The fitted fibril radius was 3.7 nm (with 50% Gaussian polydispersity), consistent with the cryo-TEM image. The SAXS data were fitted to the long core−shell cylinder model in SASfit.[48] The other fitting parameters for the results in Figure 5 are shell thickness ΔR = 0.1 nm and scattering contrast of core η(core) = −0.0075, η(shell) = 0.161, and η(solvent) = 0.0035. A flat background BG = 0.17 was included in the fit.

AFM (Supporting Information Figure 8) shows that, above cac1, but below cac2, $A_{10}H_6$ self-assembles mainly into globular prefibrillar structures; however, some fibrils are also present. The latter appear to be formed by stacks of nanometer-scale globules, suggesting that the cac2 transition is determined by a further structural rearrangement leading to mature "amyloid-like" fibrils.

X-ray diffraction also confirms a tightly packed β-sheet structure for $A_{10}H_6$ in the fibrillar state above cac2. The results shown in Figure 6 show strong peaks, corresponding to d spacings of 4.42 and 5.34 Å. As for similar alanine-rich peptides such as A_6R[49] and A_6K,[50] the former spacing is assigned as the β-strand spacing, whereas the latter is the β-sheet spacing which reflects the very close packing of β-sheets in oligo-alanine peptides.

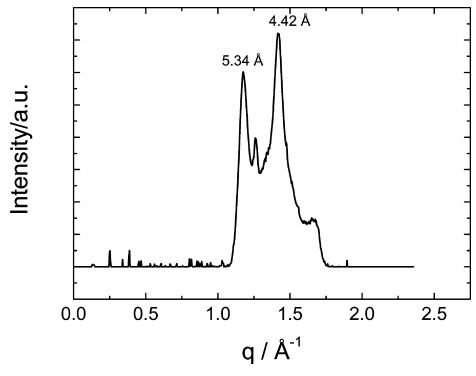

Figure 6. XRD profile obtained by integration of a fiber diffraction pattern obtained from a stalk dried from a 1 wt % solution of $A_{10}H_6$.

dx.doi.org/10.1021/bm500950c | Biomacromolecules 2014, 15, 3412−3420

Since spectroscopic methods suggest that the Nanogold particles do not influence the secondary structure of $A_{10}H_6$, we next examined the influence of the nanoparticles on the self-assembled fibril structures and potential labeling of the fibrils by Nanogold. Figure 7 presents TEM and cryo-TEM images, both

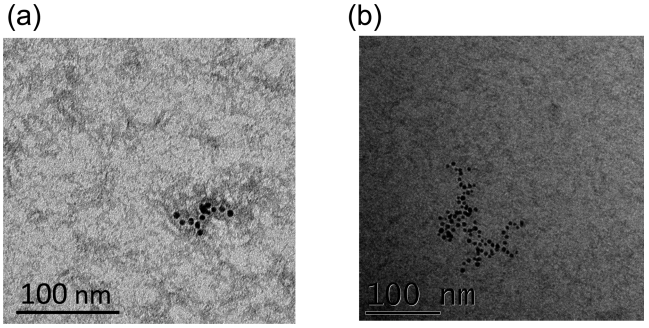

Figure 7. Electron micrographs showing interaction of Nanogold with $A_{10}H_6$ fibrils. (a) TEM image of 1.5 wt % $A_{10}H_6$ + 0.5 μM Nanogold in MOPS. (b) Cryo-TEM image of 1 wt % $A_{10}H_6$ + 0.5 μM Nanogold in MOPS.

of which clearly show the association of the Nanogold with the peptide fibrils. The $A_{10}H_6$ nanostructures are short, disperse fibrils resembling those for the peptide in the absence of Nanogold (Figure 4). This again suggests association of the gold nanoparticles with the peptide fibrils without disruption of morphology (or secondary structure, probed by spectroscopic methods). AFM also shows association of Nanogold with peptide fibrils, a representative image being presented in Figure 8. From the line cross-section scans, it can be estimated that the peptide fibrils are just under 6 nm in height, and the total height of the nanoparticles on top of the peptide is 11−12 nm. This suggests some compression of the underlying peptide when the diameter of the Nanogold particles, around 8−10 nm, is considered. The concentration of gold nanoparticles is low, so that not all fibrils were observed to be decorated with them.

Remarkably, evidence for the binding of the Nanogold to the histidine residues in the peptide could be obtained from CD spectroscopy in the range 510−530 nm, that is, in the region of the gold nanoparticle plasmon band (Supporting Information Figure 9). The CD spectrum in Figure 9 shows a substantial decrease of the negative minimum in this range by adding micromolar $A_{10}H_6$ aliquots to Nanogold. The CD signal from the functionalized gold nanoparticles is ascribed to an induced Cotton effect caused by the chiral center on the NTA chain. The linking of, for example, thiols causes a reconstruction of the gold surface with some degree of stereochemistry.[51] However, D- and L-type reconstruction is equally probable, so the result is again optical inactivity. However, when chiral molecules are linked to the gold surface, the D/L parity is removed, and the plasmon transition is optically active, gaining a net CD signal as demonstrated for peptide-tethered gold nanoparticles.[52,53] As this region of the spectrum is sensitive to the Ni^{2+}/histidine interaction,[54−56] these results clearly indicate the binding of the Nanogold to the peptide.

DISCUSSION

The aggregation process for $A_{10}H_6$ occurs via two distinct critical aggregation concentrations. We are not aware of prior reports on two-stage assembly processes for surfactant-like peptides. However, two-step aggregation processes have been

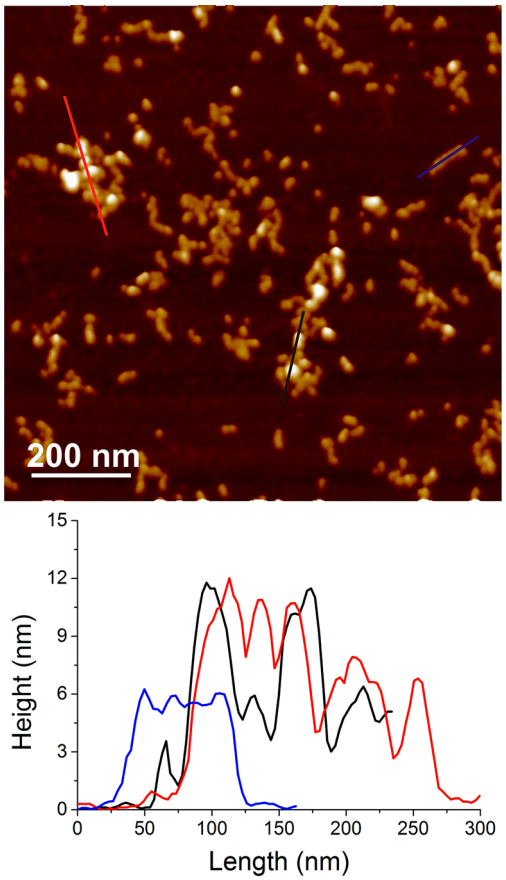

Figure 8. Top: AFM image showing Gold NPs associated with short $A_{10}H_6$ fibrils (0.5 wt % peptide concentration in MOPS). Bottom: The corresponding lines indicate cross sections.

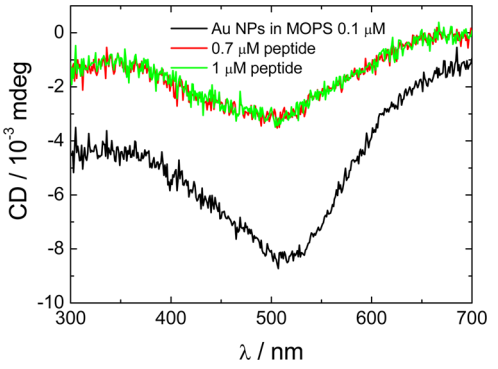

Figure 9. CD spectra showing interaction of histidine residues in $A_{10}H_6$ with gold nanoparticles, in the region of the plasmon absorption band (Supporting Information Figure 6).

observed for other amyloid-forming peptides.[57] For example, computer simulations on the amyloid β peptide fragment Aβ(16−22) show an initial step corresponding to the sequestration of hydrophobic residues within molten oligomers.[57−61] The second aggregation step corresponds to the reorganization within oligomers resulting from interchain hydrogen bonding which produces β-sheet assemblies. Hints for a similar initial hydrophobic collapse into globular oligomers followed by subsequent β-sheet formation were obtained from experiments on the related fragment Aβ(16−20).[62] It is possible that a similar mechanism occurs for the surfactant-like peptide studied herein.

dx.doi.org/10.1021/bm500950c | Biomacromolecules 2014, 15, 3412−3420

We have shown that the hexa-histidine coating of the fibrils could be used to tag the amyloid assemblies using Ni/NTA-functionalized gold nanoparticles (Nanogold). This selective tagging was shown not to influence the formation of β-sheet secondary structures formed above cac2. Intriguing effects on the gold nanoparticle Plasmon absorbance spectrum due to binding to the peptide were observed via CD spectroscopy in the visible wavelength range and our results show that the Nanogold particles are optically active, presumably due to the effect of the capping ligands. Binding to the β-sheet forming $A_{10}H_6$ peptide leads to a reduction in the negative plasmon-associated CD signal. For helical peptides, the sign of this chiral absorbance band depends in an odd−even fashion on the sequence length.[53] A detailed model for this is still lacking, also for our observation of modulation of the chiral Plasmon CD signal upon binding to a model β-sheet forming peptide.

Our work suggests that if hexa-histidine-tagged proteins misfold into amyloid structures they may be tagged using Ni-NTA gold nanoparticles. Peptide nanotubes have been coated with gold nanoparticles, and these assemblies show two-dimensional charge transport behavior within the quantum dot arrays.[63] Other applications of hybrid peptide/nanoparticle structures in sensing (using peptides immobilized on gold nanoparticles) have been discussed.[64] Our hybrid peptide/inorganic nanowire structures may also have applications where one-dimensional patterning of nanoparticles is exploited.

CONCLUSIONS

In conclusion, we have developed a model alanine-rich peptide tagged with a hexa-histidine sequence that self-assembles into amyloid fibrils. Remarkably, the aggregation process occurs via two distinct critical aggregation concentrations. The first, cac1, in the micromolar range seems to relate to the formation of mainly globular structures via an open association process. The second cac2 = 2 mM is associated with the formation of amyloid fibrils, since it was located via fluorescence using the amyloid-binding dye thioflavin T (as well as pyrene fluorescence sensitive to the local hydrophobic environment). Fibril formation above cac2 was confirmed via electron microscopy, atomic force microscopy, and small-angle X-ray scattering, and the presence of β-sheets was revealed by spectroscopic (CD and FTIR) methods as well as X-ray diffraction.

We have shown that the tagging of amyloid peptide fibrils with gold NPs enables enhanced TEM imaging. The selective tagging does not hinder the formation of β-sheet secondary structures formed above cac2. Our work suggests that incorporation of hexa-histidine tags incorporated into model peptides or recombinantly expressed proteins that adopt amyloid fibril structures is a potentially useful technique to decorate amyloid fibrils.

ASSOCIATED CONTENT

Supporting Information

Reaction schemes, characterization data, additional fluorescence and absorption spectroscopy data, AFM images, and CD spectra This material is available free of charge via the Internet at http://pubs.acs.org

AUTHOR INFORMATION

Corresponding Author

*E-mail: I.W.Hamley@reading.ac.uk.

Present Address

[†]V.C.: National Physical Laboratory, Hampton Rd, Teddington, Middlesex TW11 0LW, U.K.

Notes

The authors declare no competing financial interest.

ACKNOWLEDGMENTS

This work was supported by EPSRC Grant EP/L020599/1. S.K. is the recipient of an STFC Futures Studentship. I.W.H. acknowledges the support of a Royal Society-Wolfson Research Merit Award for work on peptide self-assembly. We are grateful to the ESRF for the award of beamtime on beamline BM29 (ref. MX-1606) and to Adam Round for assistance with the measurements. The synthesis activity was supported by ESMI (European Soft Matter Infrastructure, proposal ref S130200339).

REFERENCES

(1) Hochuli, E.; Dobeli, H.; Schacher, A. *J. Chromatogr.* **1987**, *411*, 177.
(2) Vaughan, T. J.; Williams, A. J.; Pritchard, K.; Osbourn, J. K.; Pope, A. R.; Earnshaw, J. C.; McCafferty, J.; Hodits, R. A.; Wilton, J.; Johnson, K. S. *Nat. Biotechnol.* **1996**, *14*, 309.
(3) Schmitt, J.; Hess, H.; Stunnenberg, H. G. *Mol. Biol. Rep.* **1993**, *18*, 223.
(4) Huang, Z. H.; Hwang, P.; Watson, D. S.; Cao, L. M.; Szoka, F. C. *Bioconjugate Chem.* **2009**, *20*, 1667.
(5) Zhao, C. X.; Hellman, L. M.; Zhan, X.; Bowman, W. S.; Whiteheart, S. W.; Fried, M. G. *Anal. Biochem.* **2010**, *399*, 237.
(6) Hainfeld, J. F.; Liu, W. Q.; Halsey, C. M. R.; Freimuth, P.; Powell, R. D. *J. Struct. Biol.* **1999**, *127*, 185.
(7) Acar, S.; Carlson, D. B.; Budamagunta, M. S.; Yarov-Yarovoy, V.; Correia, J. J.; Ninonuevo, M. R.; Jia, W. T.; Tao, L.; Leary, J. A.; Voss, J. C.; Evans, J. E.; Scholey, J. M. *Nat. Commun.* **2013**, *4*, 1343.
(8) Gunasekar, S. K.; Anjia, L.; Matsui, H.; Montclare, J. K. *Adv. Funct. Mater.* **2012**, *22*, 2154.
(9) Zhang, M.; Mao, X.; Yu, Y.; Wang, C.-X.; Yang, Y.-L.; Wang, C. *Adv. Mater.* **2013**, *25*, 3780.
(10) Ji, X. J.; Naistat, D.; Li, C. Q.; Orbulescu, J.; Leblanc, R. M. *Colloids Surf., B* **2006**, *50*, 104.
(11) Vannoy, C. H.; Xu, J.; LeBlanc, R. M. *J. Phys. Chem. C* **2009**, *114*, 266.
(12) Gupta, S.; Babu, P.; Surolia, A. *Biomaterials* **2010**, *31*, 6809.
(13) Bastus, N. G.; Sanchez-Tillo, E.; Pujals, S.; Farrera, C.; Kogan, M. J.; Giralt, E.; Celada, A.; Lloberas, J.; Puntes, V. *Mol. Immunol.* **2009**, *46*, 743.
(14) Shaw, C. P.; Middleton, D. A.; Volk, M.; Levy, R. *ACS Nano* **2012**, *6*, 1416.
(15) Chan, H. M.; Xiao, L. H.; Yeung, K. M.; Ho, S. L.; Zhao, D.; Chan, W. H.; Li, H. W. *Biomaterials* **2012**, *33*, 4443.
(16) Antosova, A.; Gazova, Z.; Fedunova, D.; Valusova, E.; Bystrenova, E.; Valle, F.; Daxnerova, Z.; Biscarini, F.; Antalik, M. *Mater. Sci. Eng., C* **2012**, *32*, 2529.
(17) Liao, Y. H.; Chang, Y. J.; Yoshiike, Y.; Chang, Y. C.; Chen, Y. R. *Small* **2012**, *8*, 3631.
(18) Bolisetty, S.; Boddupalli, C. S.; Handschin, S.; Chaitanya, K.; Adamcik, J.; Saito, Y.; Manz, M. G.; Mezzenga, R. *Biomacromolecules* **2014**, *15*, 2793.
(19) Kogan, M. J.; Bastus, N. G.; Amigo, R.; Grillo-Bosch, D.; Araya, E.; Turiel, A.; Labarta, A.; Giralt, E.; Puntes, V. F. *Nano Lett.* **2006**, *6*, 110.
(20) Triulzi, R. C.; Dai, Q.; Zou, J. H.; Leblanc, R. M.; Gu, Q.; Orbulescu, J.; Huo, Q. *Colloids Surf., B* **2008**, *63*, 200.
(21) Zhang, D. M.; Neumann, O.; Wang, H.; Yuwono, V. M.; Barhoumi, A.; Perham, M.; Hartgerink, J. D.; Wittung-Stafshede, P.; Halas, N. J. *Nano Lett.* **2009**, *9*, 666.

(22) Chen, A. Y.; Deng, Z.; Billings, A. N.; Seker, U. O. S.; Lu, M. Y.; Citorik, R. J.; Zakeri, B.; Lu, T. K. *Nat. Mater.* **2014**, *13*, 515.
(23) Djalali, R.; Chen, Y.-F.; Matsui, H. *J. Am. Chem. Soc.* **2002**, *124*, 13660.
(24) Aldeek, F.; Safi, N.; Zhan, N.; Palui, G.; Mattousi, H. *ACS Nano* **2013**, *7*, 10197.
(25) Hadjichristidis, N.; Iatrou, H.; Pispas, S.; Pitsikalis, M. *J. Polym. Sci., Part A: Polym. Chem.* **2000**, *38*, 3211.
(26) Mavrogeorgis, D.; Bilalis, P.; Karatzas, A.; Skoulas, D.; Fotinogiannopoulou, G.; Iatrou, H. *Polym. Chem.* **2014**, DOI: 10.1039/C4PY00687A.
(27) Gitsas, A.; Floudas, G.; Mondeshki, M.; Spiess, H. W.; Aliferis, T.; Iatrou, H.; Hadjichristidis, N. *Macromolecules* **2008**, *41*, 8072.
(28) Kalyanasundaram, K.; Thomas, J. K. *J. Am. Chem. Soc.* **1977**, *99*, 2039.
(29) Wolszczak, M.; Miller, J. *J. Photochem. Photobiol., A* **2002**, *147*, 45.
(30) Borocci, S.; Ceccacci, F.; Galantini, L.; Mancini, G.; Monti, D.; Scipioni, A.; Venanzi, M. *Chirality* **2003**, *15*, 441.
(31) Alzalamira, A.; Ceccacci, F.; Monti, D.; Mortera, S. L.; Mancini, G.; Sorrenti, A.; Venanzi, M.; Villani, C. *Tetrahedron: Asymmetry* **2007**, *18*, 1868.
(32) Berne, B. J.; Pecora, R. *Dynamic Light Scattering*; Wiley-Interscience: New York, 1976.
(33) Provencher, S. W. *Makromol. Chem.* **1979**, *180*, 201.
(34) Winnik, F. M. *Chem. Rev.* **1993**, *93*, 587.
(35) Castelletto, V.; Cheng, G.; Greenland, B. W.; Hamley, I. W. *Langmuir* **2011**, *27*, 2980.
(36) Hamley, I. W.; Dehsorkhi, A.; Castelletto, V. *Langmuir* **2013**, *29*, 5050.
(37) Castelletto, V.; Gouveia, R. J.; Connon, C. J.; Hamley, I. W.; Seitsonen, J.; Nykänen, A.; Ruokolainen, J. *Biomaterials Science* **2014**, *2*, 362.
(38) Dehsorkhi, A.; Castelletto, V.; Hamley, I. W. *J. Pept. Sci.* **2014**, *20*, 453.
(39) Link, S.; El-Sayed, M. A. *J. Phys. Chem. B* **1999**, *103*, 4212.
(40) Woody, R. W. In *Circular dichroism. Principles and applications*; Nakanishi, K. et al., Eds.; VCH: New York, 1994.
(41) Hamley, I. W. *Angew. Chem.* **2007**, *46*, 8128.
(42) Nordén, B.; Rodger, A.; Dafforn, T. R. *Linear Dichroism and Circular Dichroism: A Textbook on Polarized-Light Spectroscopy*; RSC: Cambridge, 2010.
(43) Hamley, I. W.; Nutt, D. R.; Brown, G. D.; Miravet, J. F.; Escuder, B.; Rodríguez-Llansola, F. *J. Phys. Chem. B* **2010**, *114*, 940.
(44) Stuart, B. *Biological Applications of Infrared Spectroscopy*; Wiley: Chichester, 1997.
(45) Pelton, J. T.; McLean, L. R. *Anal. Biochem.* **2000**, *277*, 167.
(46) Gaussier, H.; Morency, H.; Lavoie, M. C.; Subirade, M. *Appl. Environ. Microbiol.* **2002**, *68*, 4803.
(47) Eker, F.; Griebenow, K.; Schweitzer-Stenner, R. *Biochemistry* **2004**, *43*, 6893.
(48) http://kur.web.psi.ch/sans1/SANSSoft/sasfit.html.
(49) Hamley, I. W.; Dehsorkhi, A.; Castelletto, V. *Chem. Commun.* **2013**, *49*, 1850.
(50) Middleton, D. A.; Madine, J.; Castelletto, V.; Hamley, I. W. *Angew. Chem., Int. Ed. Engl.* **2013**, *52*, 10537.
(51) Jadzinsky, P. D.; Calero, G.; Ackerson, C. J.; Bushnell, D. A.; Kornberg, R. D. *Science* **2007**, *318*, 430.
(52) Schaaff, T. G.; Knight, G.; Shafigullin, M. N.; Borkman, R. F.; Whetten, R. L. *J. Phys. Chem. B* **1998**, *102*, 10643.
(53) Longo, E.; Orlandin, A.; Mancin, F.; Scrimin, P.; Moretto, A. *ACS Nano* **2013**, *7*, 9933.
(54) Valenti, L. E.; De Pauli, C. P.; Giacomelli, C. E. *J. Inorg. Biochem.* **2006**, *100*, 192.
(55) Klewpatinond, M.; Viles, J. H. *Biochem. J.* **2007**, *404*, 393.
(56) Zoroddu, M. A.; Medici, S.; Peana, M. *J. Inorg. Biochem.* **2009**, *103*, 1214.
(57) Cheon, M.; Chang, I.; Mohanty, S.; Luheshi, L. M.; Dobson, C. M.; Vendruscolo, M.; Favrin, G. *PLoS Comput. Biol.* **2007**, *3*, 1727.
(58) Wu, C.; Lei, H.; Duan, Y. *J. Am. Chem. Soc.* **2005**, *127*, 13530.
(59) Ellisdon, A. M.; Thomas, B.; Bottomley, S. P. *J. Biol. Chem.* **2006**, *281*, 16888.
(60) Nguyen, P. H.; Li, M. S.; Stock, G.; Straub, J. E.; Thirumalai, D. *Proc. Natl. Acad. Sci. U.S.A.* **2007**, *104*, 111.
(61) Watzky, M. A.; Morris, A. M.; Ross, E. D.; Finke, R. G. *Biochemistry* **2008**, *47*, 10790.
(62) Krysmann, M. J.; Castelletto, V.; Kelarakis, A.; Hamley, I. W.; Hule, R. A.; Pochan, D. J. *Biochemistry* **2008**, *47*, 4597.
(63) Shekhar, S.; Anjia, L.; Matsui, H.; Khondaker, S. I. *Nanotechnology* **2011**, *22*, 095202.
(64) de la Rica, R.; Matsui, H. *Chem. Soc. Rev.* **2010**, *39*, 3499.